Available online at www.sciencedirect.com
SCIENCE DIRECT®
Journal of Sound and Vibration 288 (2005) 1197–1222
JOURNAL OF SOUND AND VIBRATION
www.elsevier.com/locate/jsvi

Transmission of roll, pitch and yaw vibration to the backrest of a seat supported on a non-rigid car floor

Y. Qiu, M.J. Griffin*

Human Factors Research Unit, Institute of Sound and Vibration Research, University of Southampton, Southampton SO17 1BJ, UK

Received 7 November 2003; received in revised form 3 December 2004; accepted 27 January 2005
Available online 27 April 2005

Abstract

The transmission of roll, pitch and yaw vibration from the floor of a small car to the seat backrest has been investigated with three road conditions. At the seat base, there were distinctive differences between roll vibration at the front and rear of the seat base and between pitch vibration at the left- and right-hand side of the seat base. The yaw motion was generally small relative to the roll and pitch motion. At high frequencies, the yaw motion calculated from the difference between fore-aft vibration at the left- and right-hand side of the seat base was less than the yaw motion calculated from the differences between lateral vibration at the front and back of the seat base. Furthermore, yaw motion calculated from the difference in lateral vibration at the right-hand side of the seat was greater than that at the left-hand side, due to differences between the two lateral accelerations at the two right corners of the seat base. The measurements indicated that the seat base was not a rigid structure in either roll, pitch or yaw.

The transmission of rotational vibration from the non-rigid seat base to fore-and-aft, lateral and vertical vibration at the seat backrest was investigated using single- and multi-input models. It was found that pitch and roll vibration, together with translational vibration at the seat base, made significant contributions to seat backrest vibration. For predicting seat transmissibility in the fore-aft and vertical directions, a translational model comprising all the least-correlated fore-aft and vertical inputs, and a combined rotational and translational model consisting of the pitch vibration input and part of the least-correlated fore-aft and vertical inputs appeared equally good. Low coherency in the transmission of vibration to the

*Corresponding author. Tel.: +44 2380 592277; fax: +44 2380 592927.
E-mail address: m.j.griffin@soton.ac.uk (M.J. Griffin).

0022-460X/$ - see front matter
doi:10.1016/j.jsv.2005.01.029

lateral direction of the seat backrest observed when considering only translational vibration at the seat base was resolved after taking into account the effect of the roll vibration at the seat base.

1. Introduction

There are complex multi-axis motions on the floors of cars, with combined translational and rotational components. The vibration is transmitted through car seats and contributes to the vibration discomfort of drivers and passengers [1]. Most previous studies of the transmission of vibration through car seats have assumed a single-input model in which vertical vibration at the seat base contributes to vertical vibration at the surface supporting the seat occupant. A small number of studies have investigated the transmission of horizontal vibration from the seat base to the seat surface [2–5] but there have been a few investigations of the transmission of fore-and-aft, lateral or vertical vibration to the backrest. Using multi-input models of seat transmission, two recent studies have investigated the extent to which the fore-and-aft, lateral and vertical vibration at a car floor contributed to fore-and-aft, lateral and vertical vibration at a seat backrest [6,7]. It was found in these studies that the vibration on a car floor differed between the four corners of the seat base, implying that there were rotational (i.e. roll, pitch and yaw) inputs to the seat.

It seems reasonable to suppose that fore-and-aft vibration at the seat backrest might be induced not only by the fore-and-aft and vertical vibration at the seat base but also by pitch motion of the vehicle [6]. A study of the transmission of translational vibration to car seats using single- and two-input models found that fore-and-aft vibration at the seat base was not the only source of fore-aft vibration of the backrest and a contribution from rotational motion at the seat base was hypothesised [7].

The principal objective of the current paper is to identify the roll, pitch and yaw motion at the seat base in a small car and understand how the combined translational and rotational motion of the seat base is transmitted to the seat occupant.

2. Vibration measurements and characteristics of the input motion

2.1. Implementation of the vibration measurements

Vibration at the seat base (i.e. car floor) and the seat backrest were measured during road tests in an experimental car (Ford Mondeo, Zetec 2.0L, Y451 AOT). The car had a mass of 1372 kg and a wheelbase of 2754 mm. Tests were made in three different road conditions in and around the City of Southampton: a smooth road (a dual carriageway), a street road, and a bumpy road (rural area). Measurements were repeated three times in each road condition for each subject. Two drivers who participated in the tests weighed 80 and 70 kg and had a stature of 1.83 m and 1.70 m, respectively. Driving speed was 40 mph with the car in 4th gear. The data presented in this paper were obtained with the first driver (80 kg and 1.83 m) but the data obtained from the second driver were similar.

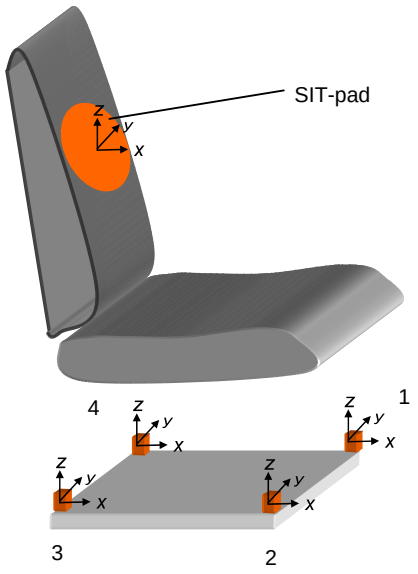

Fig. 1. Installation of SIT-pad and accelerometers on the seat and the seat base: 4 tri-axial accelerometer blocks mounted at four corners of seat base.

Fig. 1 shows how the transducers were arranged during the tests. A "SIT-pad" conforming to ISO 10326-1 [8] with built-in tri-axial accelerometers was used to measure accelerations in the fore-and-aft (i.e. x-axis), lateral (i.e. y-axis) and vertical (i.e. z-axis) directions at the seat backrest. The distance between the centre of the backrest pad and the car floor was 610 mm. Four blocks of transducers were placed at each corner of the seat base to measure acceleration at each location in the x-, y- and z-directions (Fig. 1). The four blocks were labelled 1, 2, 3 and 4 in clockwise order starting from the front left corner. Each block contained three piezoresistive accelerometers orientated in the three directions. The four blocks were mounted such that they were co-axial with the four bolts firmly pinning the seat on the car floor. In the tests, whereas accelerometers used for blocks 2, 3 and 4 were Entran EGCSY-240D-10 and Entran EGCS-DO-10/V10/L4 M types (both having acceleration range ± 10 g), the accelerometers used for block 1 were Entran EGCSY-240DO-50 type (having acceleration range ± 50 g).

Input vibration (at the seat base) and output vibration (at the seat backrest) were measured simultaneously. In the test, a total of 15 acceleration signals (3 outputs from the backrest, plus 12 inputs from the seat base) were acquired to an *HVLab* data acquisition and analysis system (version 3.81). The test duration was 60 s and acceleration was sampled at 200 samples per second via 67 Hz anti-aliasing filters.

2.2. Characteristics of the input motion at the seat base

Assume that x_i, y_i and z_i ($i = 1, 2, 3$ and 4) represent accelerations in the fore-aft, lateral and vertical directions at the four corners of the seat base (Fig. 1). Figs. 2–4 show the power spectral density functions for the acceleration measured in the three road conditions using a resolution of 0.78 Hz with 188 degrees of freedom (dofs). The frequency content of the spectra shows some

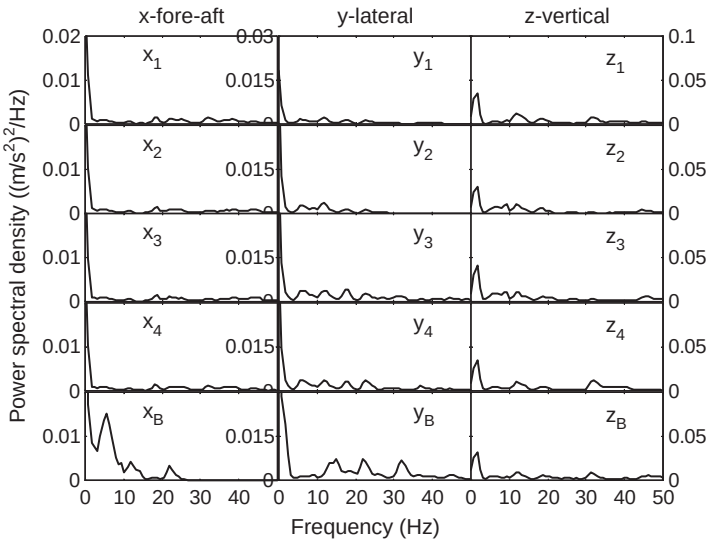

Fig. 2. Acceleration power spectral density functions measured on a smooth road, 40 mph.

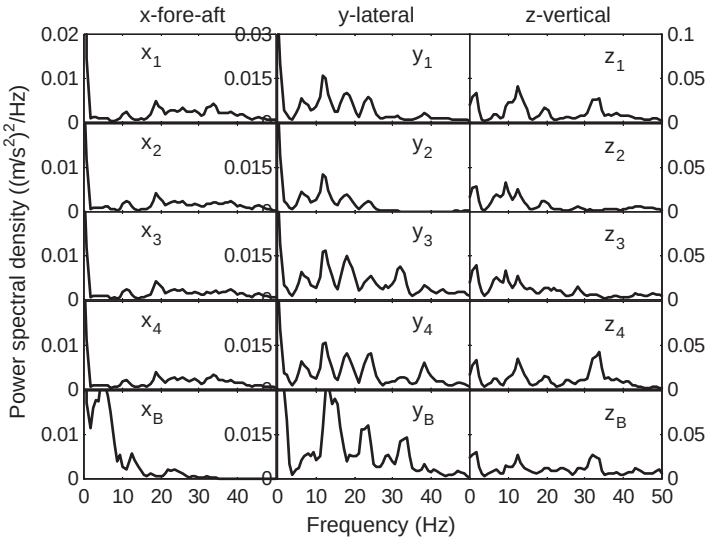

Fig. 3. Acceleration power spectral density functions measured on a street road, 40 mph.

similarity among the input signals in the same direction. For fore-aft acceleration, the four signals (x_1, x_2, x_3 and x_4) at four corners of the seat base are similar. For lateral acceleration, there is a similar situation between the front signals (y_1 and y_2) and the rear signals (y_3 and y_4). For vertical acceleration, the two accelerations (z_1 and z_4) on the left-hand side are similar and the other two on the right-hand side are similar. The above features may more easily be seen in Fig. 5 which overlays the power spectral densities of pairs of input signals at each side of the seat base in the x-, y- and z-directions for measurements over the street road.

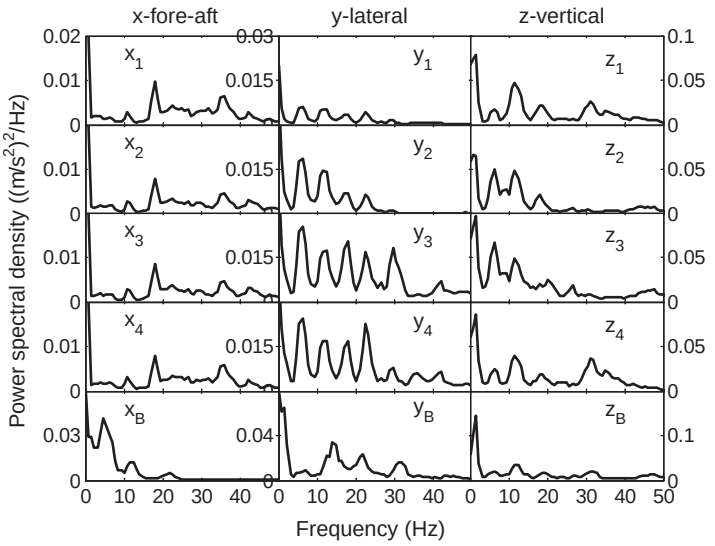

Fig. 4. Acceleration power spectral density functions measured on a bumpy road, 40 mph.

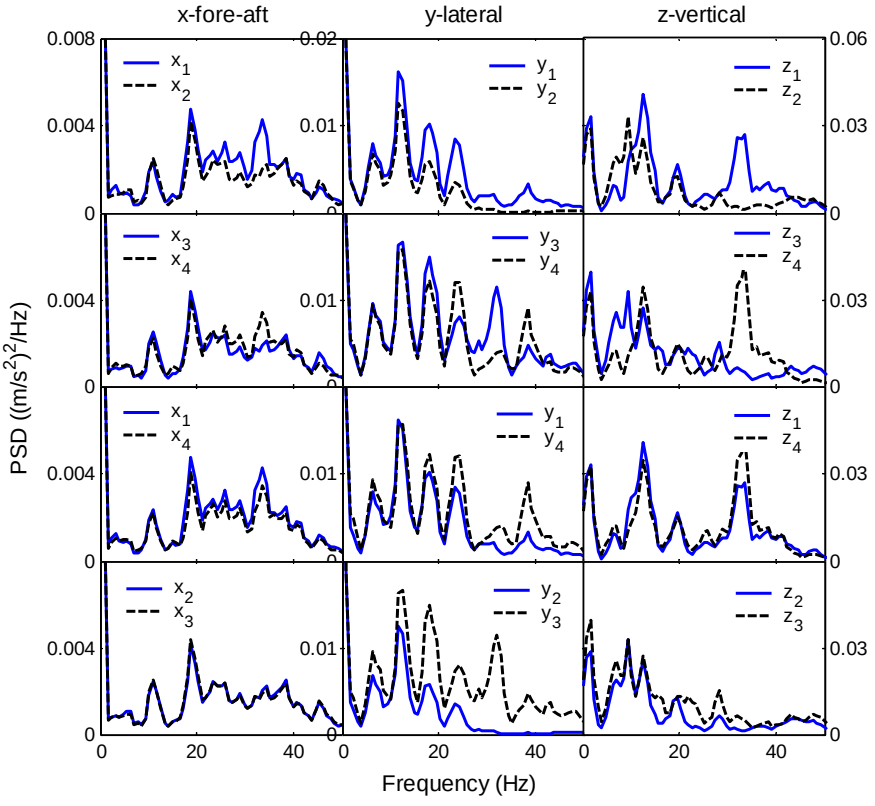

Fig. 5. Comparison of the four acceleration power spectral density functions in the fore-and-aft, lateral and vertical directions at the four corners of the seat. Measurements on a street road at 40 mph (see Fig. 1 for notation).

Although the distributions of the input accelerations from the three road conditions are not the same, some common features can be seen for the three road conditions in Figs. 2–4. In the fore-aft direction, vibration acceleration was mainly distributed over the frequency range of 5–50 Hz with a distinctive peak around 20 Hz. In the lateral direction, vibration acceleration was mostly in the frequency range 5–30 Hz (with a principal peak around 12 Hz), although the vibration extends to 50 Hz for the rear lateral acceleration (y_3 and y_4). In the vertical direction, vibration acceleration was greatest in the frequency range 2–40 Hz, with clear peaks around 2, 12 and 35 Hz.

Similar to the Ford Focus [7], the vibration of the Ford Mondeo varied from corner to corner of the seat base, as can be seen from the power spectral density functions in Figs. 2–4 for the three road conditions. Table 1 lists the acceleration rms values and frequency-unweighted vibration dose values (VDVs) computed from the measured input signals. The greatest difference is in the lateral acceleration between the rear and the front sides of the seat base, while fore-aft acceleration of the four corners shows less difference. This is visible in Fig. 5 for the street road.

Using the data obtained in the street road (Fig. 3), transfer functions between each pair of input signals in the same x-, y- or z-direction were computed, using a single-input and single-output model. Fig. 6 shows the modulus and phase angle of the transfer functions calculated between pairs of the least-correlated fore-aft accelerations at the front side (x_1 and x_2) and at the rear side (x_3 and x_4) of the seat base. The corresponding results between pairs of lateral accelerations at the left-hand side (y_1 and y_4) and at the right-hand side (y_2 and y_3) are shown in Fig. 7. In these figures, H_{ij} represents the transmissibility from the acceleration at position i to the acceleration at position j. It can be seen from Figs. 6 and 7 that the transmissibilities are non-unity, indicating that each pair of vibration inputs at the seat base differed, as also demonstrated in Fig. 5. The difference between the two fore-aft motions at the front side and at the rear side can be considered to be yaw motion for that side of the seat base. Similarly, the yaw motion at the

Table 1
The unweighted rms accelerations and frequency-unweighted vibration dose values (VDV)

Acceleration	Smooth road		Street road		Bumpy road	
	rms (m/s^2)	VDV ($m/s^{1.75}$)	rms (m/s^2)	VDV ($m/s^{1.75}$)	rms (m/s^2)	VDV ($m/s^{1.75}$)
x_1	0.242	1.097	0.361	1.501	0.422	1.659
x_2	0.228	1.062	0.321	1.319	0.389	1.537
x_3	0.226	1.046	0.322	1.325	0.390	1.539
x_4	0.229	1.059	0.330	1.387	0.398	1.559
y_1	0.204	0.854	0.480	1.903	0.302	1.160
y_2	0.256	1.027	0.408	1.593	0.485	1.823
y_3	0.320	1.298	0.569	2.238	0.667	2.573
y_4	0.316	1.297	0.558	2.307	0.643	2.468
z_1	0.495	2.270	0.748	3.165	0.874	3.286
z_2	0.446	1.819	0.628	2.587	0.818	3.071
z_3	0.530	2.267	0.759	3.130	0.992	3.728
z_4	0.503	2.324	0.782	3.330	0.915	3.468
x_b	0.369	1.506	0.452	1.786	0.497	1.941
y_b	0.437	1.954	0.698	2.790	0.638	2.417
z_b	0.508	2.309	0.766	3.306	0.652	2.437

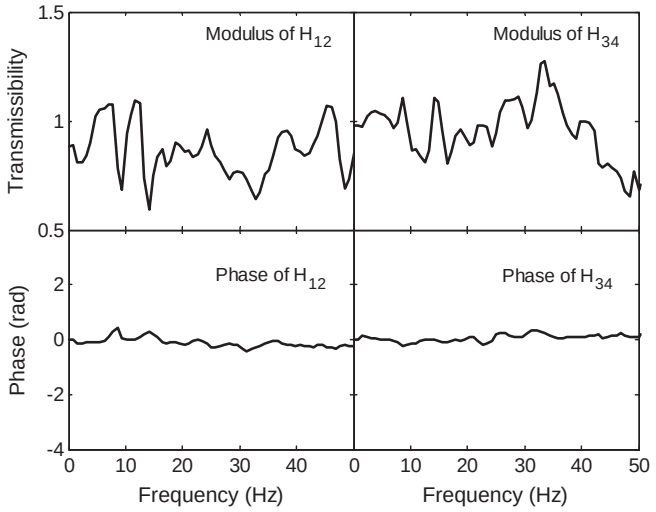

Fig. 6. Modulus and phase of the transmissibility between a pair of fore-and-aft inputs, street road, 40 mph. Subscript '12' means between fore-aft inputs at position 1 (front left corner) and at position 2 (front right corner). Subscript '34' means between fore-aft inputs at position 3 (rear right corner) and at position 4 (rear left corner).

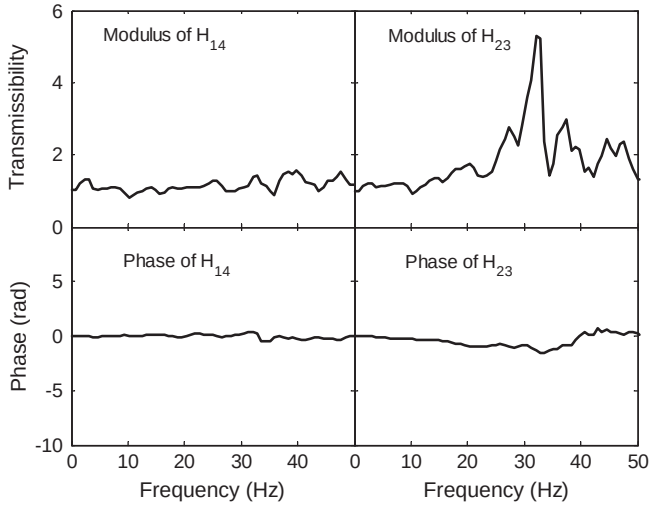

Fig. 7. Modulus and phase of the transmissibility between a pair of lateral inputs, street road, 40 mph. Subscript '14' means between lateral inputs at position 1 (front left corner) and at position 4 (rear left corner). Subscript '23' means between lateral inputs at position 2 (front right corner) and at position 3 (rear right corner).

left- and right-hand sides of the seat base can be calculated from the difference between the two lateral accelerations at the left- and right-hand side.

The accelerations in the vertical direction at the four corners of the seat base were distinct from each other, as can be seen in Fig. 5 and further demonstrated in Figs. 8 and 9. Fig. 8 shows the modulus and phase angle of the transmissibilities from pairs of vertical acceleration at the front

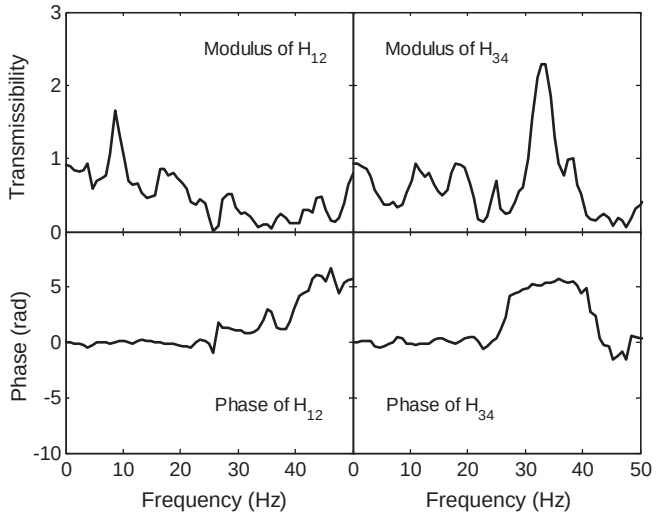

Fig. 8. Modulus and phase of the transmissibility between a pair of vertical inputs, street road, 40 mph. Subscript '12' means between vertical inputs at position 2 (front left corner) and at position 2 (front right corner). Subscript '34' means between vertical inputs at position 3 (rear right corner) and at position 4 (rear left corner).

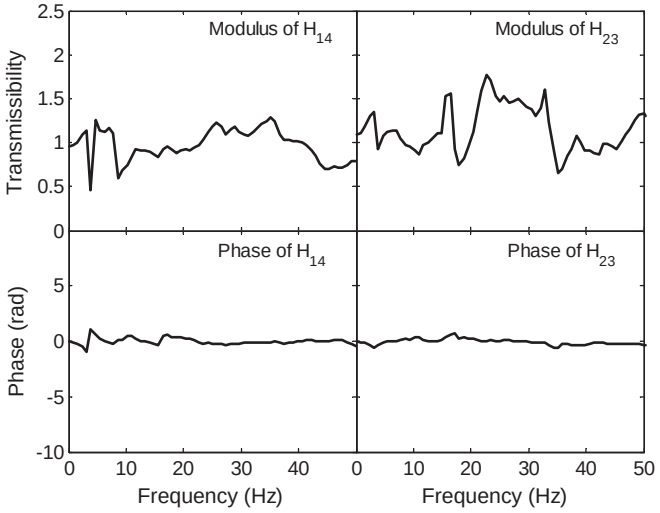

Fig. 9. Modulus and phase of the transmissibility between a pair of vertical inputs, street road, 40 mph. Subscript '14' means between vertical inputs at position 1 (front left corner) and at position 4 (rear left corner). Subscript '23' means between vertical inputs at position 2 (front right corner) and at position 3 (rear right corner).

(z_1 and z_2) and the rear (z_3 and z_4). The differences between these pairs of vertical accelerations correspond to roll motions at the front and the rear of the seat base. The transmissibilities from pairs of vertical acceleration at the left-hand side (z_1 and z_4) and at the right-hand side (z_2 and z_3) are shown in Fig. 9. The differences between these pairs of vertical accelerations correspond to pitch motion at the left- and right-hand side of the seat base.

In the following section, roll, pitch and yaw motion at the seat base will be calculated based on the translational motions measured at the four corners of the seat base as described above.

3. Roll, pitch and yaw motion at the seat base

The traditional approach to studying the transmission of vibration through a car seat is to assume the seat base is a rigid body. With this assumption, complete motion of the seat base is fully defined by 6 dofs: three translational motions (x, y and z, usually measured at the centre of the seat base) and three rotational motions (θ_x, θ_y and θ_z): fore-aft, lateral, vertical, roll, pitch and yaw vibration. It would be sufficient to consider vibration sources associated with the above six axes when studying seat transmissibility if the seat base is rigid.

It has been found in the current study that the seat base at the car floor does not always behave rigidly. This situation is now discussed by considering the rotational motions of the seat base associated with the differences in translational vibration at the four corners of the seat base (see Fig. 10).

While pitch motion is induced by a difference in the vertical motion of the seat base between the front and the rear, the difference in vertical motion between the left- and right-hand side will cause roll motion. The roll and pitch accelerations at the edges of the seat base can be computed based on the vertical accelerations of the seat base:

$$\text{Roll, front}: \ \theta_x^{\text{front}} = \frac{z_1 - z_2}{d} \ (\text{rad/s}^2),$$
$$\text{Roll, rear}: \ \theta_x^{\text{rear}} = \frac{z_4 - z_3}{d} \ (\text{rad/s}^2), \tag{1}$$

$$\text{Pitch, right}: \ \theta_y^{\text{right}} = \frac{z_3 - z_2}{l} \ (\text{rad/s}^2),$$
$$\text{Pitch, left}: \ \theta_y^{\text{left}} = \frac{z_4 - z_1}{l} \ (\text{rad/s}^2). \tag{2}$$

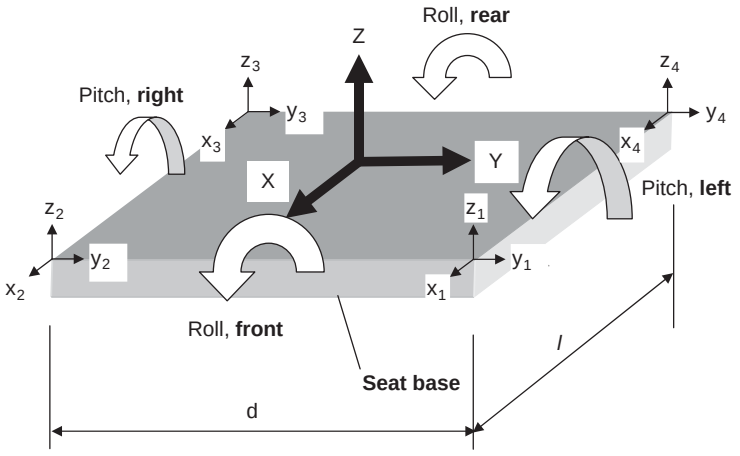

Fig. 10. Rotational motions in the seat base.

In a similar manner, yaw accelerations for the four edges of the seat base are computed based on the fore-aft and lateral accelerations:

$$\begin{aligned}
\text{Yaw, right}: \ \theta_z^{\text{right}} &= \frac{y_2 - y_3}{l} \ (\text{rad/s}^2),\\
\text{Yaw, left}: \ \theta_z^{\text{left}} &= \frac{y_1 - y_4}{l} \ (\text{rad/s}^2),\\
\text{Yaw, front}: \ \theta_z^{\text{front}} &= \frac{x_2 - x_1}{d} \ (\text{rad/s}^2),\\
\text{Yaw, rear}: \ \theta_z^{\text{rear}} &= \frac{x_3 - x_4}{d} \ (\text{rad/s}^2).
\end{aligned} \tag{3}$$

In the above equations, d and l represent the width and depth of the seat base (Fig. 10). Having computed the roll, pitch and yaw motions in the time domain, their corresponding power spectral density functions $G_{\theta_x^{\text{front}}}(f)$, $G_{\theta_x^{\text{rear}}}(f)$, $G_{\theta_y^{\text{right}}}(f)$, $G_{\theta_y^{\text{left}}}(f)$, $G_{\theta_z^{\text{right}}}(f)$, $G_{\theta_z^{\text{left}}}(f)$, $G_{\theta_z^{\text{front}}}(f)$ and $G_{\theta_z^{\text{rear}}}(f)$ are then obtained via signal processing.

Furthermore, the relative difference in roll motion is defined in the frequency domain as the absolute difference between the power spectral densities of the front- and the rear-roll relative to the power spectral density of the front roll:

$$\Delta G_{\theta_x}(f) = \frac{|G_{\theta_x^{\text{rear}}}(f) - G_{\theta_x^{\text{front}}}(f)|}{G_{\theta_x^{\text{front}}}(f)}. \tag{4}$$

The relative difference in the pitch motion is defined as the absolute difference between the power spectral densities of the right- and the left-pitch relative to the power spectral density of the left pitch:

$$\Delta G_{\theta_y}(f) = \frac{|G_{\theta_y^{\text{right}}}(f) - G_{\theta_y^{\text{left}}}(f)|}{G_{\theta_y^{\text{left}}}(f)}. \tag{5}$$

Similarly, two relative differences in yaw motion between the rear- and the front-yaw, $\Delta G_{\theta_z^{rf}}(f)$, and between the right- and the left-yaw, $\Delta G_{\theta_z^{rl}}(f)$, can be calculated:

$$\begin{aligned}
\Delta G_{\theta_z^{rf}}(f) &= \frac{|G_{\theta_z^{\text{rear}}}(f) - G_{\theta_z^{\text{front}}}(f)|}{G_{\theta_z^{\text{front}}}(f)},\\
\Delta G_{\theta_z^{rl}}(f) &= \frac{|G_{\theta_z^{\text{right}}}(f) - G_{\theta_z^{\text{left}}}(f)|}{G_{\theta_z^{\text{left}}}(f)}.
\end{aligned} \tag{6}$$

If the seat base is rigid, the relative difference in rotational motion should be sufficiently small to be considered zero. Therefore, the relative difference in rotational motion is an indicator of the non-rigidity of the seat base. Based on Eqs. (1)–(6), the roll, pitch, yaw and their relative differences at the seat base were computed for the three road conditions.

3.1. Roll motion

Roll spectra at the front ($G_{\theta_x^{\text{front}}}(f)$) and the rear ($G_{\theta_x^{\text{rear}}}(f)$) of the seat base are shown in Fig. 11 for the three road conditions. From Fig. 11, the power spectral density of the roll motion at the

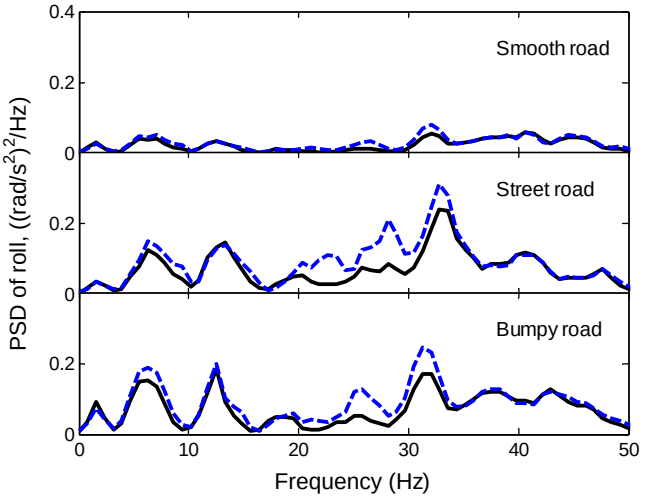

Fig. 11. Comparison of the front and rear roll motions for three road conditions: —— front roll; – – – rear roll.

front of the seat base had similar frequency components to that at the rear of the seat base. The vibration acceleration is primarily centred around 6, 12 and 33 Hz. With increasing severity of the road condition, the roll motion increased. Power spectral densities of the two roll motions are close at low and high frequencies but a difference is obvious at frequencies between 20 and 35 Hz. This is true for all three road conditions, but the difference between the two roll motions is more apparent with the street road and the bumpy road than for the smooth road.

The relative difference in roll motion computed by Eq. (4) is shown in Fig. 12. The difference is mainly distributed over the frequency range between 0 and 40 Hz, over which four distinctive peaks were found around 9, 16, 22 and 28 Hz.

3.2. Pitch motion

A similar pattern was observed for the pitch motion at the seat base (Figs. 13 and 14). As can be seen from Fig. 13, the pitch motions at the two sides of the seat base had a similar frequency structure. Vibration acceleration spreads over a wide range of frequencies (up to 50 Hz) with five distinctive peaks at around 3, 10, 16, 21 and 33 Hz. Power spectral densities of the two pitch motions are similar at low frequencies but differ at high frequencies. With the more severe the road condition, there was greater pitch motion and a more obvious difference between the two pitch motions.

The pitch motions at the two sides appear to be different. The relative difference of pitch motion computed by Eq. (5) is shown in Fig. 14. The results show that the relative difference in pitch motion is greater at high frequencies than at low frequencies.

3.3. Yaw motion

Yaw motions, calculated from pairs of fore-aft motions at the front side (front yaw) and the rear side (rear yaw) of the seat base, and from pairs of lateral motions at the left-hand side (left

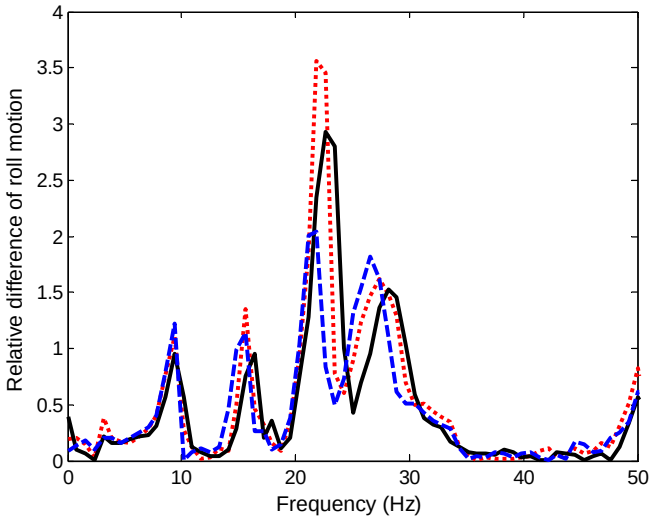

Fig. 12. Difference of the rear and front roll motion relative to the front: • • • • • • smooth road; —— street road; – – – bumpy road.

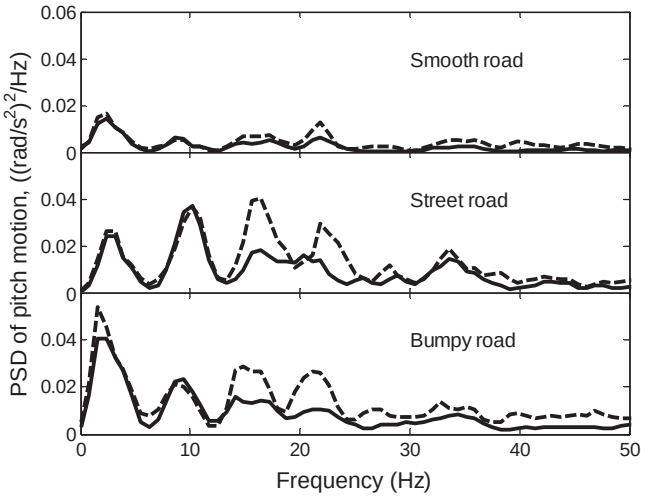

Fig. 13. Comparison of the left and right pitch motions for three road conditions: —— left pitch; – – – right pitch.

yaw) and the right-hand side (right yaw), are shown in Fig. 15. It appears that yaw motion increased with increasing severity of road condition. While the yaw motion calculated from fore-aft vibration was low, the yaw motion calculated from lateral vibration was relatively large. Of the two yaw motions calculated from the lateral motions of the seat base, the yaw motion at the right-hand side (right yaw) is higher than that at the left-hand side (left yaw). This situation is more obvious with higher magnitude inputs (street and bumpy road conditions). The effect is due to the lateral acceleration at the front right corner (y_2) of the seat base being less (especially at

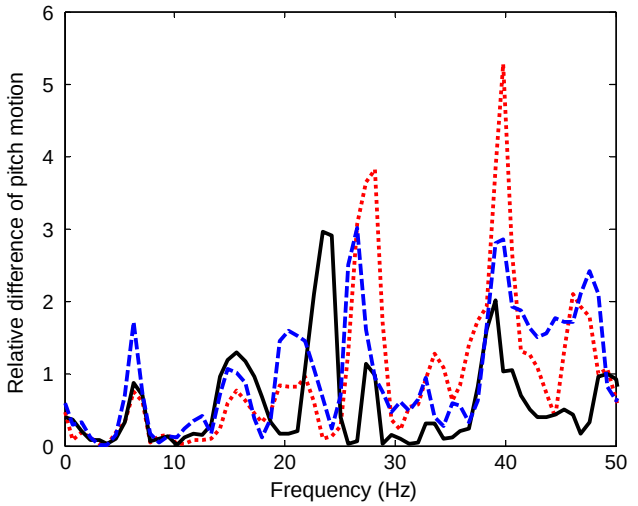

Fig. 14. Difference of the left and right pitch motion relative to the left: •••••• smooth road; —— street road; – – – bumpy road.

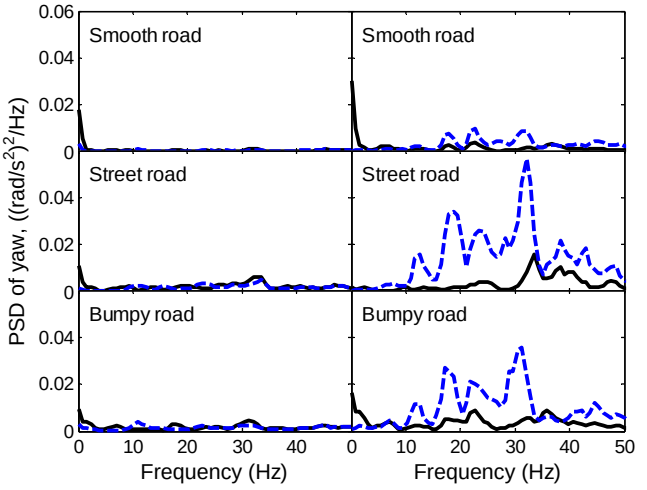

Fig. 15. Comparison of two yaw motions for each road condition: left figures, —— front yaw, – – – rear yaw; right figures, —— left yaw, – – – right yaw.

frequencies above 30 Hz) than that at the rear right corner (y_3), as can be seen in Figs. 3 and 5 for the street road. A similar finding was observed in a parallel study with a Ford Focus [7] and was also seen in a multi-body vehicle dynamics simulation for a sport utility vehicle travelling on a rough road at 50 mph. To ensure the transducers functioned correctly, a post check of the accelerometers was carried out: the 12 accelerometers were simultaneously excited by broadband random vertical vibration on an electrodynamic vibrator table: all 12 accelerometers gave values

consistent with the calibration accuracy (<3%). In addition, stationarity of the data was also checked using a run test [7] and the results suggested that the hypothesis of stationarity could be accepted for all signals ($p>0.05$). In the field tests the transducer blocks were secured to the seat rail with metal on metal contact. Any error in measuring lateral signals y_2 and y_3, could only be due to looseness between welded parts or cross-axis error in the transducers, although typical cross-axis sensitivity for the Entran accelerometers is about 2% and the motions in other axes seem unlikely to have caused errors at the frequencies where the difference in yaw was greatest. To understand why the right yaw is distinctive in this car requires inspection of the floor pan in future work.

Apart from the yaw motion implied by differences in lateral vibration, it can be seen in Fig. 15 that the yaw motion at the front and rear of the seat base is rather small compared with the roll and pitch motions (Figs. 11 and 13). This is consistent with the stiffness of the car floor being greater in yaw than in roll and pitch. Fig. 16 shows the relative difference in yaw motion calculated from differences in fore-aft vibration. The vibration energy of the relative yaw motion is mainly distributed over a frequency range 10–30 Hz with three distinctive peaks around 11, 17 and 23 Hz.

The above analysis for rotational motion shows that there were appreciable differences in roll motion (between front and rear) and pitch motion (between left and right) of the seat base. It may therefore be necessary to treat the seat base as a non-rigid body. In which case, the motion of the seat base cannot be represented simply by three rotational motions (roll, pitch and yaw) and three translational motions (x, y and z). It seems that in order to fully assess the vibration transmission from a non-rigid seat base, the vibration must be measured at each of the supports of the seat (the four corners in this case) rather than at a single convenient point on the car floor.

How are the translational and rotational motions of the seat base transmitted through the seat? This is investigated in the remainder of this paper using motions measured on the street road (Fig. 3).

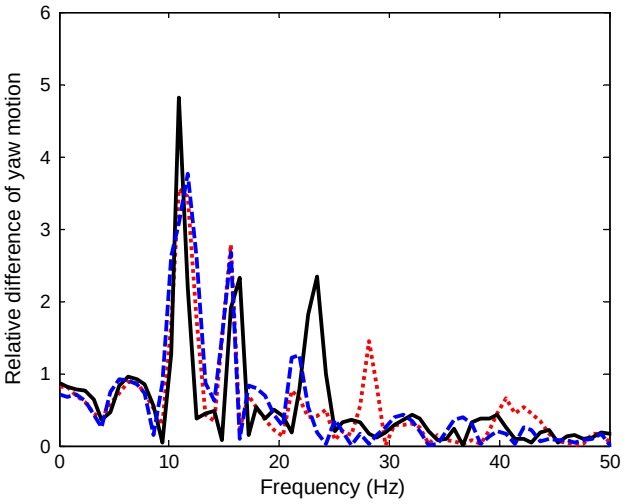

Fig. 16. Difference between the front and rear yaw motion relative to the front: •••••• smooth road; —— street road; – – – bumpy road.

4. Seat transmissibility with rotational motion using a multiple input model

Seat transmissibility, measured from the individual components of rotational motion to the translational motion of the backrest is first investigated using a single-input and single-output model. The transmissibility from the combined translational and rotational motion of the seat base is then studied with multiple-input and single-output models.

4.1. Multi-input model and computational procedure

The general multi-input and single-output model for the original seat inputs is shown in Fig. 17, whereas an alternative conditioned multi-input and single-output model is shown in Fig. 18. In these figures, the terms $X_i(f)$, $i = 1, 2, \ldots, n$, are Fourier transforms computed from the original input signals $x_i(t)$. The terms $X_{i.(i-1)!}(f)$, $i = 1, 2, \ldots, n$, represent Fourier transforms corresponding to the conditioned inputs $x_{i.(i-1)!}(t)$. For any i, the subscript notation $i.(i-1)!$ represents the ith record conditioned on the previous $(i-1)$ records, that is, when the linear effects of $x_1(t)$, $x_2(t)$, up to $x_{i-1}(t)$ have been removed from $x_i(t)$ by optimum linear least-squares prediction techniques. Note that these ordered conditioned input signals are mutually uncorrelated. $H_{iy}(f)$ and $L_{iy}(f)$ (to be determined) are constant-parameter linear frequency response functions (transfer functions) for the original and the conditioned inputs, respectively. $N(f)$ represents the Fourier transform of the unknown independent output noise and $Y(f)$ is the Fourier transform of the output signal $y(t)$. Detailed descriptions of the general multi-input single-output model and how to compute the transfer functions and ordinary and partial coherence functions can be found in Bendat and Piersol [9].

A procedure for computing the vibration transmission of a multi-input and single-output model is shown in Fig. 19. Based on this procedure, a computer programme was developed using MATLAB (version 5.3). The programme has a modular structure and consists of 12 modules with each individual module representing a single-input and single-output model (after signal conditioning). The vibration transmission of an n-input and single-output model can be realised by calling n modules one after another via a master programme.

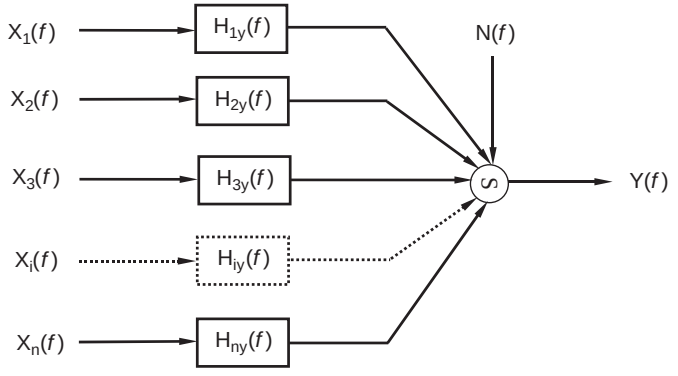

Fig. 17. Multi-input and single-output model for original inputs.

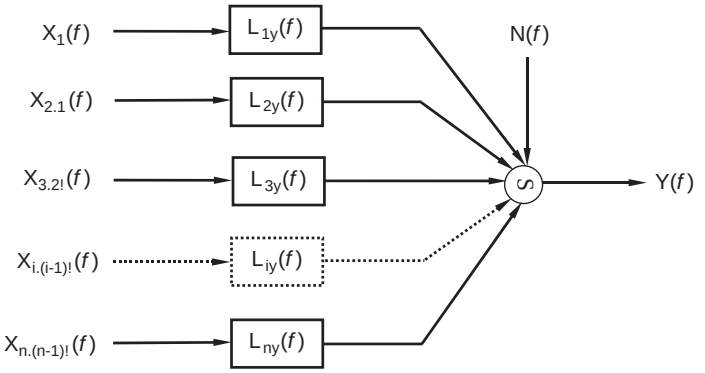

Fig. 18. Multi-input and single-output model for ordered conditioned inputs.

4.2. Transmission of pitch motion to fore-aft vibration at the seat backrest

4.2.1. From left or right pitch at the seat base to the fore-aft motion of the backrest: single-input and single-output model

A single-input and single-output model was employed to compute the seat transmissibility from an individual pitch motion (either at the left-hand side or at the right-hand side of the seat base) to fore-aft motion at the backrest. The results are shown in Fig. 20. The high coherency at some frequencies suggests that the pitch motion of the seat base made a significant contribution to the fore-aft vibration at the backrest. The primary peak in the transmissibility, especially with the right pitch motion, was at about 5 Hz. Nevertheless, the ordinary coherency for both cases was generally low, as can be seen in Fig. 20.

4.2.2. From fore-aft, vertical and pitch motion at the seat base to fore-aft motion at the backrest: six-input and one-output model

It was found in previous studies with a different car that both the fore-aft and vertical vibration of the seat base contributed to fore-aft motion at the seat backrest [6,7]. In a similar manner to the previous study [7], the backrest transmissibility from the translational inputs can be computed using a six-input model involving six translational inputs (the two least-correlated fore-aft motions and four vertical motions) at the seat base and a good multiple coherency was observed. It was expected that the multiple coherency would be further improved if the pitch motion at the seat base were taken into account.

The use of an eight-input model by simply adding two pitch motions to the above six-input model would cause a problem as the eight inputs contain redundant information. The effect of vertical motion on the seat transmissibility is partially included in the two pitch motions, since the pitch motion at one (left or right) side of the seat base was computed from the difference of the two vertical motions at that side ($(z_4–z_1)$ or $(z_3–z_2)$) via Eq. (2). Only two vertical inputs, each of which should be from a different pair of the vertical motions above, are independent of the two pitch motions. Among the four fore-aft motions at the seat base, the pair of input signals x_1 and x_4 on the left-hand side and the other pair of signals x_2 and x_3 on the right-hand side were highly correlated with each other. This means that each pair of fore-aft inputs contain redundant

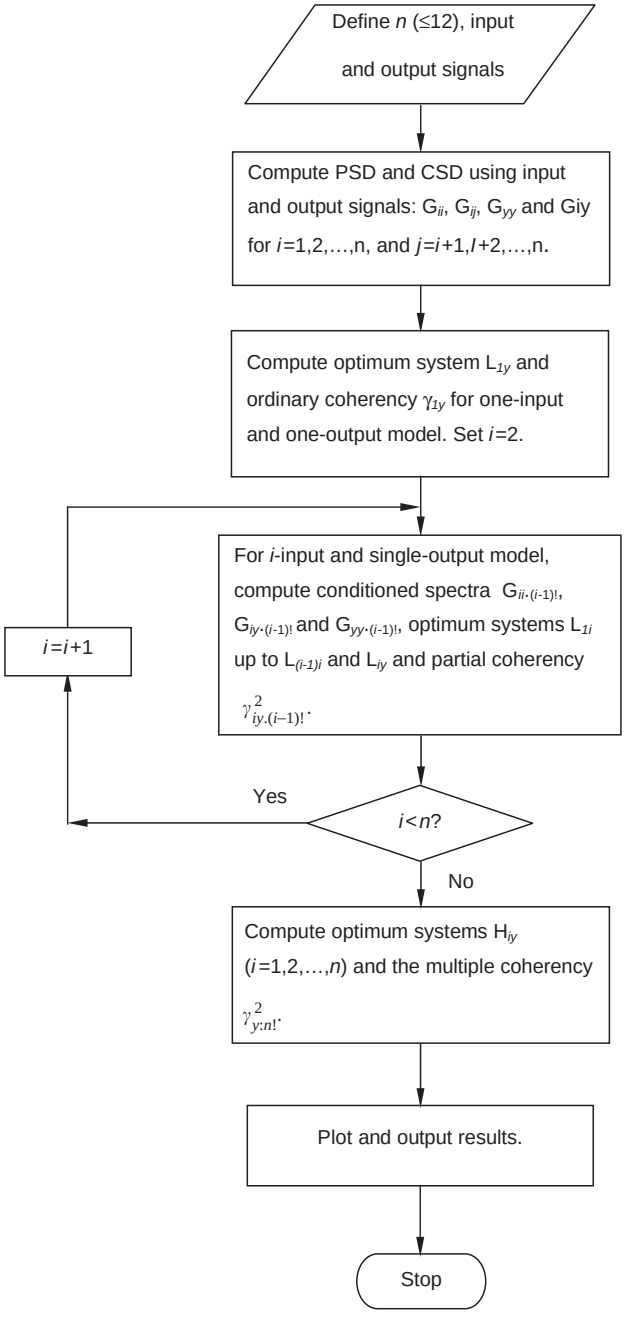

Fig. 19. Computational procedures for multi-input and single-output model.

information and that one in each pair of inputs should be excluded from the model in order to allow the distributed input systems to be studied as discrete inputs. With this in mind, to compute the transmission of vibration to the fore-aft direction on the seat backrest induced by combined

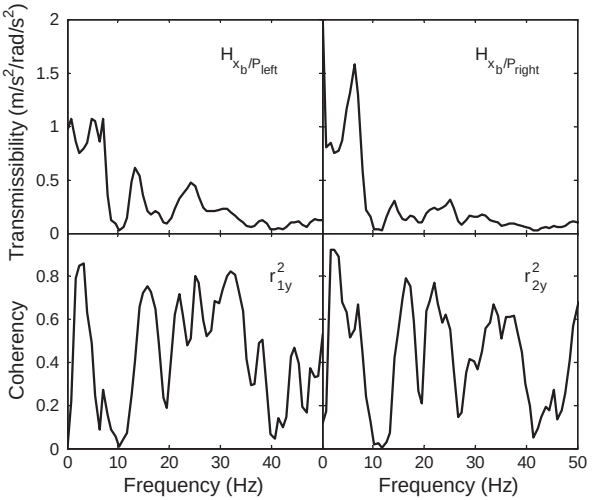

Fig. 20. Seat transmissibility and coherency from left and right pitch to the fore-aft motion of the backrest: single-input and single-output model.

translational and rotational motions on the seat base, a six-input and one-output model was formed with the six inputs in order as: the vertical motion at the rear right corner, z_3, the vertical motion at the front left corner, z_1, the left pitch, the fore-aft motion at the front left corner, x_1, the right pitch, and the fore-aft motion at the rear right corner, x_3. The six inputs were ordered according to the ordinary coherence functions between each input signal and the output signal in descending order over the frequency range of interest [7]. The computational results are shown in Figs. 21 and 22. From the transmissibilities in Fig. 21, it is seen that the primary peaks of the transmissibilities all appeared at a frequency between 4 and 6 Hz. It is confirmed from the partial coherence functions in Fig. 22 that pitch, fore-aft and vertical motions at the seat base all contributed to the backrest vibration in the fore-aft direction. An excellent multiple coherency was observed with the six-input and one-output model.

Comparing with the results from the earlier mentioned six-input model involving only translational inputs, it is not surprising to see that the multiple coherency from the two cases coincide, as shown in Fig. 23. This confirms that the effect of vertical motion on the seat transmissibility was partially included in the two pitch motions. Therefore, the effect of the pitch motion on the transmission of vibration to the backrest in the fore-aft direction with a non-rigid seat base can be taken into account by including either the four vertical vibrations or the two pitch motions plus two independent vertical motions at the seat base in the input of the model. The two treatments appear equally satisfactory.

4.3. Transmission of roll motion to lateral vibration at the seat backrest

4.3.1. From front or rear roll at the seat base to lateral motion at the backrest: single-input and single-output model

The transmission of roll motion at the seat base to lateral vibration at the backrest was calculated using a single-input and single-output model. The transmissibility and coherency from

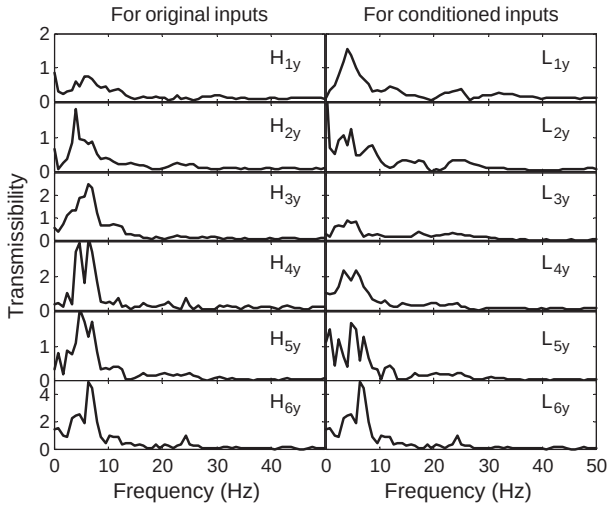

Fig. 21. Seat transmissibilities for original and conditioned inputs, from pitch, fore-aft and vertical motion at the seat base to the fore-aft motion of the backrest, six-input and one-output model.

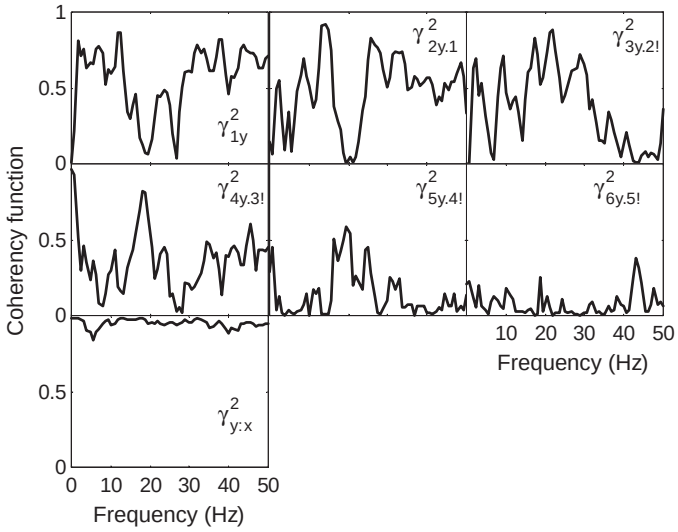

Fig. 22. Ordinary, partial and multiple coherencies, from pitch, fore-aft and vertical motion at the seat base to the fore-aft motion of the backrest, six-input and one-output model.

roll motion at the front edge of the seat base and the rear edge of the seat base to the lateral motion of the backrest is shown in Fig. 24. The transmissibility to the lateral motion of the backrest from the roll motion exhibited a rather low primary resonance at around 2 Hz.

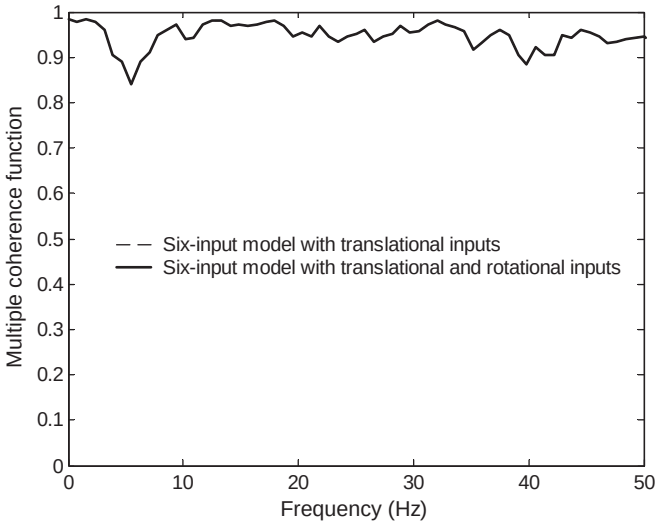

Fig. 23. Comparison of multiple coherencies for backrest transmissibility in the fore-and-aft direction obtained from a six-input model using translational inputs (z_3, z_1, x_1, x_3, z_4 and z_1) with multiple coherencies obtained from a six-input model using combined translational and rotational inputs (z_3, z_1, left pitch, x_1, right pitch and x_3): – – – six-input model with translational inputs; —— six-input model with translational and rotational inputs. (*Note*: the two coherencies are coincident).

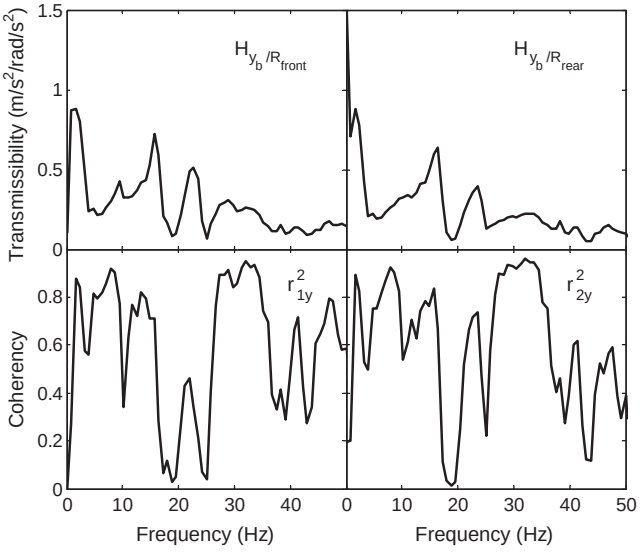

Fig. 24. Seat transmissibility and coherency from front or rear roll to the lateral motion of the backrest: single-input and single-output model.

4.3.2. From roll and lateral vibration at the seat base to lateral motion at the backrest: four-input and one-output model

In a previous study, a two-input model was used to compute seat transmissibility from the two least-correlated lateral motions at the seat base to lateral motion at the backrest [7]. The coherency was low when only considering lateral vibration at the seat base.

In this study, a four-input and one-output model was used to investigate the combined effect of roll and lateral motion at the seat base on vibration at the backrest in the lateral direction. Two lateral motions, y_1 at the front left corner and y_3 at the rear right corner, were considered since it was found that the two lateral motions at the front edge of the seat base (and another two at the rear edge of the seat base) were highly correlated. In a similar manner as mentioned in Section 4.2.2, the four inputs were ordered as rear roll, front roll, lateral motion y_3 and y_1.

The computed transmissibilities and coherencies are shown in Figs. 25 and 26. The multiple coherency was very much improved compared to the counterpart from the two-input model involving only two lateral inputs at the seat base. The comparison is shown in Fig. 27. It appears that the low coherency in the previous study was resolved after taking into account the effect of the roll motion at the seat base. The results show that the lateral vibration of the backrest was not only caused by lateral vibration but also induced by the roll motion of the seat base.

4.4. Transmission of pitch motion to vertical vibration at the seat backrest

In a similar manner to Section 4.2, the transmission of pitch vibration to vertical motion at the backrest was investigated using single- and six-input models.

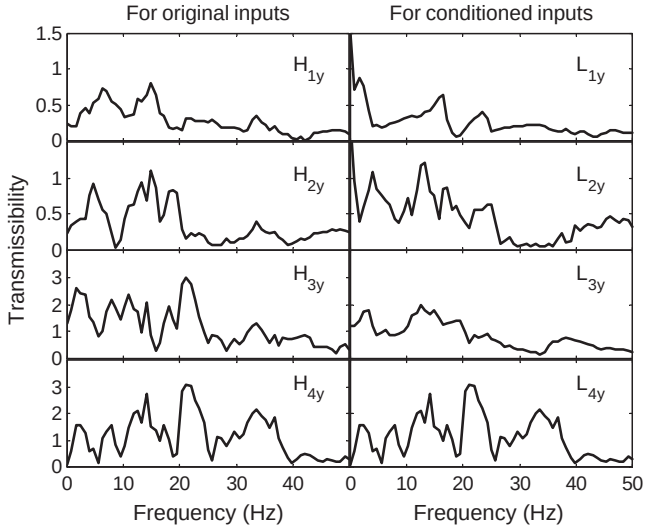

Fig. 25. Seat transmissibilities for original and conditioned inputs, from roll and lateral vibration at the seat base to the lateral motion of the backrest, four-input and one-output model.

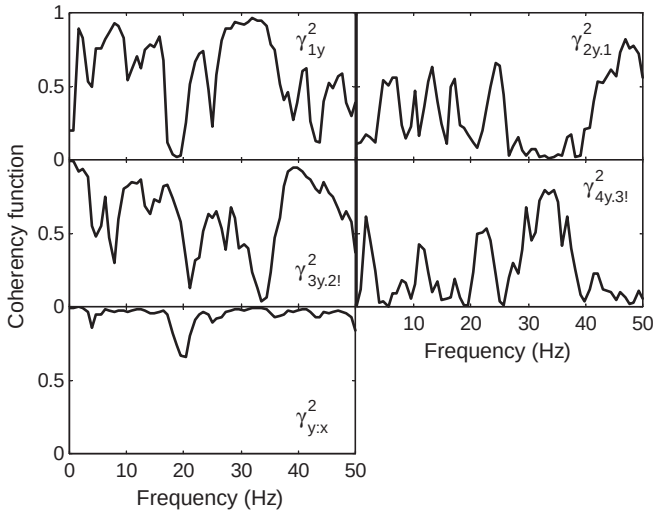

Fig. 26. Ordinary, partial and multiple coherencies, from roll and lateral vibration at the seat base to the lateral motion of the backrest, four-input and one-output model.

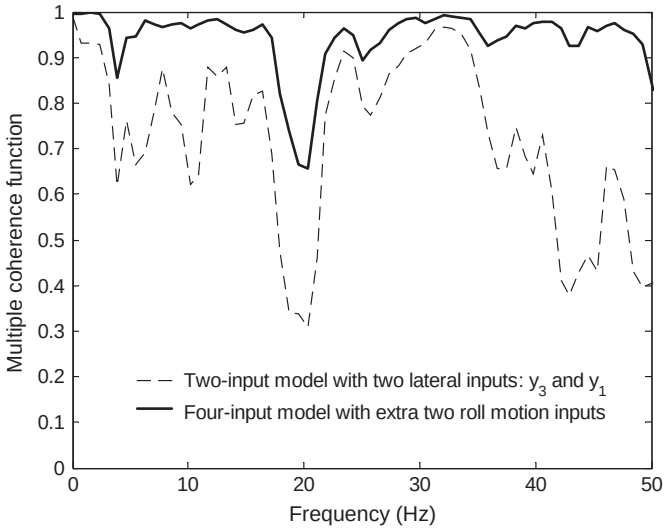

Fig. 27. Comparison of multiple coherencies for the backrest transmissibility in the lateral direction obtained from a two-input model with two lateral inputs (y_3 and y_1) with multiple coherencies obtained from a four-input model with two additional roll input motions (rear roll, front roll, y_3 and y_1): – – – two-input model with lateral inputs y_3 and y_1; —— four-input model with two additional roll motion inputs.

4.4.1. From left or right pitch at the seat base to vertical motion at the backrest: single-input and single-output model

Results using a single-input and single-output model are shown in Fig. 28. It can be seen that both the right and left pitch motions of the seat base contributed to the vertical motion of the backrest. Again, coherency was low as observed in other single-input results presented above.

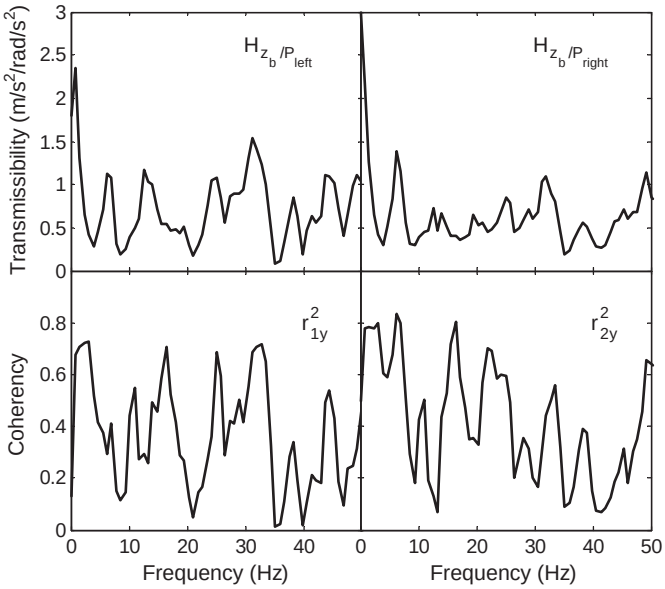

Fig. 28. Seat transmissibility and coherency from left or right pitch to the vertical motion of the backrest: single-input and single-output model.

4.4.2. From pitch, vertical and fore-aft motion at the seat base to vertical motion at the backrest: six-input and one-output model

A six-input model was used to study the transmission of pitch, vertical and fore-aft motions of the seat base to vertical motion at the backrest. The six inputs were in turn: the two vertical motions (z_3 and z_1), the pitch vibration at the right-hand side of the seat base, the fore-aft vibration at the front left corner (x_1), the pitch vibration at the left-hand side of the seat base, and the fore-aft vibration at the rear right corner (x_3) of the seat base.

The transmissibilities and coherency functions are shown in Figs. 29 and 30. The partial coherence functions in Fig. 30 show that pitch motions, and fore-aft and vertical vibration at the seat base all contributed to the vertical vibration of the backrest. Excellent multiple coherency (almost unity) was observed with the current six-input and one-output model, indicating that input sources had been very well taken into account.

Again, as found with the transmission of pitch motion to fore-aft vibration at the seat backrest, the multiple coherency from the current six-input model (combined rotational and translational inputs) is the same as that from the six-input model with six translational inputs (z_4, z_3, x_1, z_1, z_2 and x_3), as shown in Fig. 31. This suggests that for studying the transmission to vertical vibration at the backrest, similar to the case of vibration transmission to the fore-aft direction on the backrest, a model with inputs comprising two pitch and four least-correlated vertical and fore-aft (combined rotational and translational) motions at the seat base or a model whose inputs consist of six least-correlated vertical and fore-aft translational motions at the seat base are equally suitable.

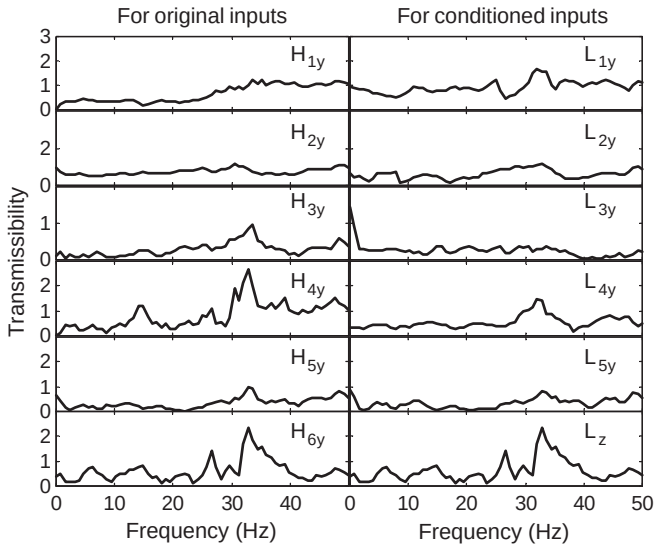

Fig. 29. Seat transmissibilities for original and conditioned inputs, from pitch, vertical and fore-aft motion at the seat base to the vertical motion of the backrest, six-input and one-output model.

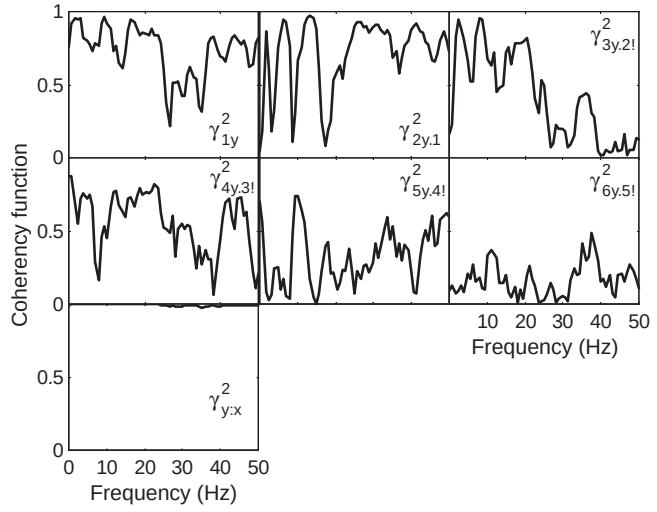

Fig. 30. Ordinary, partial and multiple coherencies, from pitch, vertical and fore-aft motion at the seat base to the vertical motion of the backrest, six-input and one-output model.

5. Conclusion

Measurements of roll, pitch and yaw motions at the base of a seat in a car showed that rotational vibration varied from position to position. It was concluded that the seat base did not

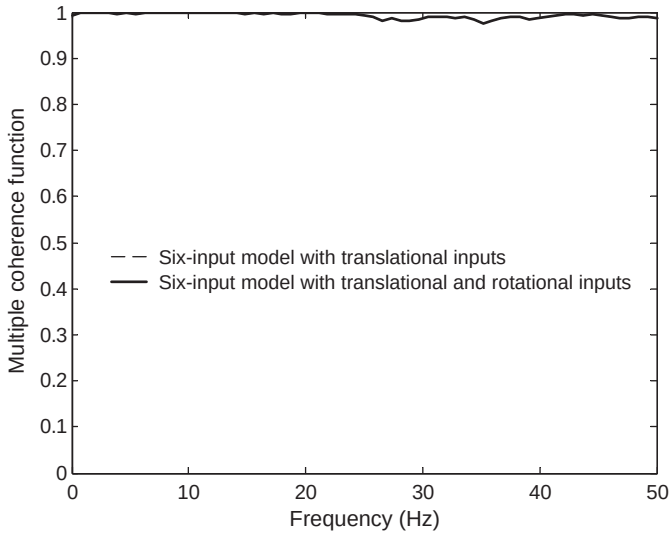

Fig. 31. Comparison of multiple coherencies for backrest transmissibility in the vertical direction obtained from a six-input model using translational inputs (z_4, z_3, x_1, z_1, z_2 and x_3) with multiple coherencies obtained from a six-input model using combined translational and rotational inputs (z_3, z_1, right pitch, x_1, left pitch and x_3): – – – six-input model with translational inputs; —— six-input model with translational and rotational inputs. (*Note*: the two coherencies are coincident).

behave as a rigid body at frequencies of interest. It therefore seemed that a full understanding of the transmission of vibration to the seat would involve consideration of the vibration at the four corners of the seat base rather than at a single point.

The transmission of pitch motion at the seat base to fore-aft motion of the seat backrest was compared using a single- and six-input model. The single-input model showed an expected peak in the transmissibility at about 5 Hz when using either the left pitch or the right pitch as the input, but the coherence was low at most frequencies. The six-input model showed that pitch, fore-aft and vertical motions at the seat base all contributed to fore-and-aft backrest vibration and a high multiple coherency was obtained. A similar strategy was used to investigate the transmission of vibration to the vertical motion of the backrest and similar results were obtained with an extremely high multiple coherency when using the six-input model. It was found that with a non-rigid car floor, equally good models for vibration transmission to the fore-and-aft and vertical motions of the backrest can be obtained with either: (i) all the relevant and uncorrelated fore-aft and vertical (translational) input motions, or (ii) the pitch motion and the remaining uncorrelated fore-aft and vertical (combined rotational and translational) inputs.

To compute the seat transmissibility between roll motion at the seat base and lateral vibration at the backrest, a single-input model gave a rather low first resonance at about 2 Hz. The combination of roll and lateral vibration at the seat base using a four-input model showed that it is not sufficient to consider only the lateral vibration at the seat base when computing seat transmissibility in the lateral direction. The lateral vibration of the backrest was caused by both the lateral motion and the roll motion of the seat base.

Acknowledgements

This research was funded by the Ford Motor Company Ltd. The authors would like to acknowledge the support of Jon Willey, Martin Jansz and Neil Dixon.

References

[1] M.J. Griffin, *Handbook of Human Vibration*, Academic Press, London, 1996.
[2] J.D. Leatherwood, National Aeronautics and Space Administration, Vibrations transmitted to human subjects through passenger seats and considerations of passenger comfort, NASA Technical Note TN D-7929, 1975.
[3] M.J. Griffin, The evaluation of vehicle vibration and seats, *Applied Ergonomics* 9.1 (1978) 15–21.
[4] C.C. Smith, Y.K. Kwak, Identification of the dynamic characteristics of a bench-type automotive seat for the evaluation of ride comfort, *Journal of Dynamic Systems, Measurement and Control* 100 (1978) 42–49.
[5] T.E. Fairley, Predicting the Dynamic Performance of Seats, Ph.D. Thesis, University of Southampton, 1986.
[6] Y. Qiu, M.J. Griffin, Transmission of fore-aft vibration to a car seat using field tests and laboratory simulation, *Journal of Sound and Vibration* 264 (1) (2003) 135–155.
[7] Y. Qiu, M.J. Griffin, Transmission of vibration to the backrest of a car seat evaluated with multi-input models, *Journal of Sound and Vibration* 274 (1–2) (2004) 297–321.
[8] International Organization for Standardization, Mechanical vibration—laboratory method for evaluating vehicle seat vibration—Part 1: basic requirements, International Standard, ISO 10326-1, 1992.
[9] J.S. Bendat, A.G. Piersol, *Random Data Analysis and Measurement Procedures*, second ed., Wiley, New York, 1986.